On modeling a rolling wheel in the presence of plastic deformation as a three- or two-dimensional process

J.P. Hambleton and A. Drescher*

Department of Civil Engineering, University of Minnesota, 500 Pillsbury Drive SE, Minneapolis, MN 55455, USA

Abstract

This paper compares predictions of deformation and horizontal (drag) force resulting from three- and two-dimensional numerical simulation of a torque-free (towed) wheel operating on ductile material. The finite element code ABAQUS/Explicit is used to simulate a complete process beginning with wheel indentation and ending, if admissible, with steady rolling. The wheel is rigid, and the material is modeled as elastic-perfectly plastic with the von Mises yield condition, with focus on plastic rather than elastic effects. It is shown that two-dimensional analysis of a rolling wheel cannot readily be applied to a narrow wheel to predict wheel penetration, although horizontal forces from three- and two- dimensional simulations follow a similar trend. In particular, it is observed that steady-state penetration is constant over a range of applied vertical forces in the two-dimensional analysis, whereas steady-state penetration is an increasing function of vertical force for narrow wheels simulated in three dimensions. This illustrates potential errors in simplifying wheel rolling by utilizing two-dimensional analysis and the necessity of considering a fully three-dimensional process. In the paper, the latter is investigated in detail.

Keywords: Rolling wheel; Three-dimensional; Plastic; Finite element method; Penetration; Force

* Corresponding author. Tel.: +1-612-625-2374; fax: +1-612-626-7750.
E-mail addresses: dresc001@umn.edu (A. Drescher), hamb0025@umn.edu (J.P.Hambleton).

List of symbols

Roman symbols

b	wheel width
$\bar{b}$	dimensionless wheel width ($\bar{b} = b / r$), i.e., wheel aspect ratio
E	Young's modulus
$\bar{E}$	dimensionless Young's modulus ($\bar{E} = E / k$)
h	projected (chord) length of contact between material and wheel (Fig. 1a)
$\bar{h}$	dimensionless contact length ($\bar{h} = h / r$)
H	horizontal component of wheel force
$\bar{H}$	dimensionless horizontal wheel force ($\bar{H} = H / kbr$)
k	shear yield stress ($k = \sigma_0 / \sqrt{3}$, where σ_0 is uniaxial yield stress)
q	average normal stress over projected length of contact ($q = Q / hb$, Fig. 1a)
$\bar{q}$	dimensionless average normal stress ($\bar{q} = q / k$)
Q	resultant force ($Q = \sqrt{W^2 + H^2}$)
r	wheel radius
u	horizontal wheel displacement
$\bar{u}$	dimensionless horizontal wheel displacement ($\bar{u} = u / r$)
W	vertical component of wheel force
$\bar{W}$	dimensionless vertical wheel force ($\bar{W} = W / kbr$)
x,y	Cartesian coordinates (Fig. 7b)

Greek symbols

α contact angle at material-wheel interface (Fig. 8b)

β angle of inclination of resultant force from vertical (Fig. 1a)

δ wheel penetration

$\bar{\delta}$ dimensionless wheel penetration ($\bar{\delta} = \delta / r$)

μ coefficient of dry friction at material-wheel interface

ν Poisson's ratio

θ angular coordinate (Fig. 9)

σ_n normal contact stress (Fig. 9)

σ_t shear contact stress (Fig. 9)

1. Introduction

Theoretical modeling and physical testing of the interaction between a rolling wheel and supporting bed of material fall within the interest of contact mechanics (cf. [1]). In many practical applications, applied wheel forces are so large as to induce primarily plastic deformation. Such areas include metal forming [2-4], rutting in asphaltic pavements [5] and unpaved roads [6,7], evaluation of vehicle mobility in soils and snow [8-12], and assessment of vehicle-induced destruction of land [13]. In some of these applications, a chief objective is to predict wheel penetration for applied vertical force (weight on wheel), torque, wheel geometry, material properties, and contact properties at the material-wheel interface. Penetration prediction is central in recently investigated

approaches for determining material properties over large areas [14,15]. In this inverse problem, the record of penetration resulting from rolling a wheel over a surface may be translated to a log of *in situ* material properties, as opposed to the single, local measurement obtained with traditional methods utilizing indenters or penetrometers.

Rolling of a wheel over a bed of material is a process. In the initial phase, the wheel comes into contact with the material, and this can be regarded as normal or oblique indentation. Subsequently, the wheel is subject to a combination of prescribed horizontal velocity, torque, horizontal force, or rotational velocity at specified vertical force (force control) or penetration (kinematic control). The movement of the wheel and the corresponding recoverable and permanent deformations depend on material properties, magnitude of applied forces, and contact properties at the material-wheel interface. In general, the wheel may reach a steady state of motion at some limited penetration, or it may sink and bury itself in the material.

Observations indicate that deformation induced by the narrow wheels of typical vehicles and mobile machinery is clearly three-dimensional. This greatly hampers modeling efforts, especially when the material response is nonlinear. Two-dimensional solutions therefore have been suggested as viable alternatives, and in addition to providing first order approximations, they provide valuable reference [18-27]. Three-dimensional analyses have only recently been proposed [7,11,12,14-17,28].

This paper attempts to theoretically analyze the process of a narrow wheel rolling over plastically deforming material, with emphasis on three-dimensional effects. Two-dimensional (plane strain) rolling of a cylinder is considered for comparison. In both cases the analysis is based on extensive numerical simulations using the finite element

method (FEM). Flexibility of the wheel is disregarded, and the wheel is taken to be rigid. Also, the potentially complex geometry of a wheel is simplified to a right-cylinder. The material deforming beneath the rolling wheel is assumed to be elastic-plastic (no rate effects), and the process of rolling is quasi-static (no inertial effects). The analysis is limited to wheels with no driving torque, i.e., free-rolling wheels that are towed or pushed. Effects of repeated loading are not considered.

Simulations described in this paper pertain to materials exhibiting pressure-independent yielding according to the classical associated flow theory of plasticity. Materials obeying this constitutive model include ductile metals and saturated clays under undrained conditions. This simple material model is used for consistence with previous studies [14,15,21,22], although constitutive laws representing other types of materials may be implemented [7,11-12,16-17].

The three-dimensional simulation methods employed to analyze the rolling process were originally developed in previous works [14-17]. In extension of these works, this paper focuses on differences arising between three- and two-dimensional models, particularly the potential errors ensuing from the assumption of two-dimensionality. Detailed analysis of the contact area and stresses at the material-wheel interface are also provided in this paper. This analysis highlights basic similarities and differences between three- and two-dimensional rolling processes, as well as the similarity between steady rolling and indentation processes.

2. Material and numerical models

Material in contact with the rolling rigid wheel was modeled as isotropic and elastic-perfectly plastic, with linear elasticity (Young's modulus E; Poisson's ratio ν) and plasticity governed by the von Mises yield condition (shear yield stress $k = \sigma_0/\sqrt{3}$, where σ_0 is uniaxial yield stress) with associated (incompressible) plastic flow. Dry friction with coefficient of friction μ and shear stress limit k was prescribed as the contact interaction between the material and wheel. The material was assumed to be weightless, although it was verified that introducing unit weight does not noticeably affect the results.

The geometry of the wheel is defined by two variables: radius r and width b. The vertical (i.e., normal) and horizontal (i.e., tangential or longitudinal) components of force acting at the wheel's center of rotation are denoted W and H, respectively. As the wheel is torque-free, W and H are the only forces present. Vertical penetration of the wheel is denoted δ (Fig. 1). In presenting and interpreting the results, the following dimensionless variables are used:

$$\bar{\delta} = \frac{\delta}{r}, \quad \bar{b} = \frac{b}{r}, \quad \bar{W} = \frac{W}{kbr}, \quad \bar{H} = \frac{H}{kbr}, \quad \bar{E} = \frac{E}{k} \tag{1}$$

Normalized width $\bar{b}$ is also referred to as "aspect ratio," and this parameter is typically in the range $0.2 \le \bar{b} \le 0.6$ for mobile machinery. Note that $\bar{W}$ and $\bar{H}$ in Eq. (1) represent forces per unit wheel width. Force per unit width in the two-dimensional (plane strain) simulations are used interchangeably with the ratios W/b and H/b appearing in Eq. (1).

The two-dimensional configuration is denoted by $\bar{b} = \infty$, as the plane strain condition is exact for an infinitely wide cylinder.

The effects of elasticity and contact friction do not play a central role in the results presented in this paper. That is, it was confirmed that the same basic findings regarding plastic flow around a rolling wheel apply for varying values of $\bar{E}$, ν, and μ, with the exception of the scenario $\bar{E} \to 0$ which degenerates to the purely elastic problem. Simulations were performed using $\bar{E} = 700$ and $\nu = 0.3$, which are representative of soft metals and geomaterials. The coefficient of friction was $\mu = 0.5$.

As described in previous papers [14-17], the rolling process was simulated using the commercial FEM software ABAQUS/Explicit. Compared to implicit schemes, the explicit time integration used in ABAQUS/Explicit is particularly efficient in tracing the highly nonlinear solution path present in the rolling process, which arises due to large, plastic deformation and contact interactions at the material-wheel interface. Remeshing capabilities for correcting element distortions, via the Arbitrary Lagrangian-Eulerian (ALE) method, are also provided in ABAQUS/Explicit [29]. The code is dynamic, although a quasi-static solution is obtained through slow and smooth application of boundary conditions.

The bed of deforming material was represented by a prismatic (rectangular for two-dimensional simulations) body of length 20*r*, depth 5*r* and width 8-12*r* discretized using linear 8-node hexahedral elements (4-node quadrilaterals in two dimensions) with reduced integration and hourglass control. Element length in the region of material contacting the wheel was roughly 0.05*r*. Three-dimensional simulations took advantage of the plane of symmetry at the wheel midplane, and only one half of the full material

domain and wheel was therefore simulated. The right-cylindrical wheel was modeled as an analytical rigid surface [29], meaning that it was a smooth, non-discretized surface with rigid body displacements and forces specified at a single reference node. A fillet of radius $b/20$ was used at the wheel edge to avoid numerical difficulties in the contact algorithm. The material was partitioned into strong and weak regions in order to replicate a realistic process by which a wheel enters a region prone to significant penetration. The yield strength k in the strong region was taken four times that in the weak region, such that $\overline{E} = 175$ in the strong region. In some simulations, a homogeneous bed of material with $\overline{E} = 700$ was modeled.

Simulation consisted of three stages. In the first stage, the vertical force W was applied to the wheel while it was placed on the region of relatively strong material. Next, horizontal velocity at the wheel's center was ramped smoothly from zero to a prescribed value. In the final stage, the wheel rolled into the region of relatively weak material with constant W and horizontal velocity, being free to displace vertically (penetrate an amount δ) and rotate through frictional interaction with the material surface. Zero wheel torque about the wheel's axis of rotation was specified in the second and third stages.

As the results presented in this paper derive from numerical simulation, inherent errors arise due to spatial and time discretizations. Also, inertial effects are present with the particular code used, and the process must be simulated over sufficiently large time for quasi-static conditions to apply. These issues were not explored in detail for this paper; however, simulation parameters affecting numerical error (e.g., element length, size and number of time steps, remeshing increment, etc.) were chosen based on a previous work [14] in which satisfactory accuracy was demonstrated.

3. Wheel rolling

Figure 2a shows normalized penetration $\bar{\delta}$ (plotted positive downward) as a function of $\bar{u}$ for several values of $\bar{W}$, where $\bar{u} = u/r$ and u is horizontal wheel displacement. The value of $\bar{\delta}$ at $\bar{u} = 0$ is the penetration resulting from normal indentation while the wheel is positioned over the region of strong material ($\bar{E} = 175$). While the wheel is over this region, deformation is largely elastic. The dashed line at $\bar{u} = 0.25$ indicates the position at which the center of the wheel passes directly over the boundary between strong and weak material. For $1.7 \le \bar{W} \le 4.3$ in the figure, there is clearly a transient regime in which $\bar{\delta}$ varies with $\bar{u}$ (e.g., $0 \le \bar{u} \le 3$ for $\bar{W} = 2.6$), and beyond some value of $\bar{u}$, $\bar{\delta}$ becomes constant with increasing $\bar{u}$ (i.e., $d\bar{\delta}/d\bar{u} = 0$). The value of $\bar{u}$ after which $\bar{\delta}$ becomes constant tends to increase as $\bar{W}$ increases. As shown in Fig. 2b, normalized horizontal force $\bar{H}$ follows a similar pattern, with $\bar{H}$ being noisier data than $\bar{\delta}$ as a result of its higher order in the displacement-based finite element formulation.

Values of $\bar{\delta}$ and $\bar{H}$ corresponding to $d\bar{\delta}/d\bar{u} = d\bar{H}/d\bar{u} = 0$ are said to be steady, with $\bar{u}$ replacing time in the conventional definition of steadiness for the quasi-static problem. For $\bar{W}$ exceeding some value (e.g., $\bar{W} = 5.8$ in Fig. 2), no steady state exists and unstable penetration occurs in the sense that $\bar{\delta}$ continually increases with increasing $\bar{u}$.

The evolution of $\bar{\delta}$ and $\bar{H}$ with $\bar{u}$, as shown in Fig. 2, is of course affected by the magnitude of the difference in material properties in indentation (strong material) and in rolling (weak material). However, qualitatively similar behavior was also observed in

simulations with homogenous material, with penetration in the indentation phase larger than in Fig. 2a. In particular, it was verified that $\bar{\delta}$ and $\bar{H}$ in steady state were the same whether there was a strong-to-weak transition or the material was homogenous.

Figure 3a shows $\bar{\delta}$ as a function of $\bar{u}$ with varying wheel aspect ratio $\bar{b}$ and fixed $\bar{W}$. For comparison, the response when the wheel becomes an infinitely wide cylinder ($\bar{b} = \infty$) is superimposed. In the indentation phase with predominantly elastic deformation ($\bar{u} = 0$), $\bar{\delta}$ increases slightly as the wheel becomes wider. In the transient phase, different behavior can be observed for various $\bar{b}$. For the narrowest wheel ($\bar{b} = 0.2$), $\bar{\delta}$ increases monotonically before steady state is reached. For wider wheels, increasing $\bar{\delta}$ is followed by decreasing $\bar{\delta}$ in the transient phase, with steady-state $\bar{\delta}$ decreasing with an increase in $\bar{b}$. For $\bar{b} = \infty$, $\bar{\delta}$ in the steady state is close to zero, being in fact less than in the (elastic) indentation phase.

The influence of aspect ratio on normalized steady-state penetration is plotted for $\bar{W} = 2$ in Fig. 3b, where a dashed line is included to indicate that $\bar{\delta}$ becomes nearly zero as $\bar{b} \to \infty$. The analogous curve for indentation [16], with the same material properties as the weak material in the rolling simulation ($\bar{E} = 700$), is also shown. While steady-state $\bar{\delta}$ decreases monotonically as a function of $\bar{b}$ for rolling, it increases monotonically for indentation (with $\bar{\delta} \to 0.025$ as $\bar{b} \to \infty$).

One might expect that penetration, for the same vertical force, should be greater for a steady rolling wheel than an indenting wheel. As illustrated for $\bar{b} < 0.6$ in Fig. 3b, this is indeed true for narrow wheels, and the authors previously attributed this behavior to the decreased contact area and horizontal force present in rolling as compared to

indentation [14-17]. The reversal occurring as the wheel width increases can be ascribed to the tendency for material to accumulate in front of a wide wheel rather than flow to the sides. The added accumulation resulting from an increase in wheel width is shown in Fig. 4, which compares the deformation resulting for a narrow wheel and wide wheel with fixed $\bar{W}$ and $\bar{u}$. The volume of material ahead of the wide wheel is clearly much larger than the volume ahead of the narrow wheel. The face visible in the lower left represents the midplane, or plane of symmetry, of the full configuration, and the dashed line shows the position of the boundary between strong and weak materials. The wheel, while it is computationally smooth, is represented by a faceted surface in the figure. The narrow wheel in Fig. 4a has reached steady state, whereas the wide wheel in Fig. 4b is climbing ($d\bar{\delta}/d\bar{u} < 0$) and would reach steady state at larger $\bar{u}$ if in fact a steady state exists for the applied vertical force.

The relationship between $\bar{\delta}$ in the steady state and $\bar{W}$ is plotted in Fig. 5a for varying $\bar{b}$. This was obtained by constructing lines through individual points, each obtained from a single simulation where a steady state existed for the applied vertical force. The dotted line in Fig. 5a approximates the location of a boundary separating steady rolling from unstable wheel penetration, showing an increase in the threshold value of $\bar{W}$ for decreasing $\bar{b}$. The figure reveals that the behavior noted in Fig. 3a for a particular value of $\bar{W}$ applies for other values as well. That is, steady-state $\bar{\delta}$ increases as $\bar{b}$ decreases when $\bar{W}$ is held constant. Figure 5b depicts the variation of steady-state $\bar{H}$ as a function of $\bar{W}$ in steady rolling, showing that $\bar{H}$ increases with decreasing $\bar{b}$ for fixed $\bar{W}$.

A key feature of Fig. 5a is that, irrespective of $\bar{W}$, steady-state $\bar{\delta}$ becomes very small as $\bar{b}$ tends towards infinity and the two-dimensional problem. This degenerate behavior is not visible in Fig. 5b, where the dependence of $\bar{H}$ on $\bar{W}$ does not qualitatively change as $\bar{b}$ varies. The behavior and the response curves for an infinitely wide cylinder are analyzed in the next section.

4. Cylinder rolling

In this section, results of rolling an infinitely wide cylinder ($\bar{b} = \infty$, plane strain) are discussed in detail. This problem has attracted much attention in the literature both in the elastic and fully plastic steady regimes [1]. In the latter, when the material is treated as rigid-perfectly plastic, there is lack of uniqueness in the solution, for the geometry of the surface in contact with the wheel in steady state is unknown beforehand (cf. [22]).

As argued in the literature (cf. [30,31]), the shape of the surface in problems dealing with steady plastic flow may result from (1) the loading history or (2) through minimization of dissipated energy (i.e., “minimum effort” hypothesis). On the other hand, numerical simulations of the whole rolling process as described in this paper appear devoid of this ambiguity, with the resulting shape of the free surface determined uniquely. Petryk [31] suggested, on the basis that a solution with minimal energy is stable against small perturbations, that the minimum energy principle plays a larger, if not exclusive role over the loading history in determining the physically most likely solution among an infinity of admissible solutions. It may be said further based on results of the numerical simulations described in this paper that initial conditions do not seem to play a

role in determining the steady-state configuration for a rolling wheel, as the same steady state was reached for particular wheel loading and material parameters regardless of how the indentation phase was simulated.

Figure 6a shows $\bar{\delta}$ as a function of $\bar{u}$ for $\bar{b} = \infty$ and various values of $\bar{W}$. With increasing $\bar{W}$, the wheel penetrates deeper when rolled onto the weak material and then climbs up and slightly rolls down to a constant penetration corresponding to steady state. A steady state again exists provided $\bar{W}$ is not so large as to induce unstable penetration (e.g., $\bar{W} \geq 2.6$ in Fig. 6a). Figure 6b gives the dependence of $\bar{\delta}$ and $\bar{H}$ on $\bar{W}$ in steady state. For small $\bar{W}$, when elasticity dominates, the steady state penetration is nearly a linear function of $\bar{W}$. For relatively large $\bar{W}$ corresponding to primarily plastic deformation, $\bar{\delta}$ is constant, while $\bar{H}$ strictly increases. It should be noted as in the previous section that $\bar{\delta}$ is quite small overall. The non-zero penetration occurring in the predominately plastic regime is in fact due to minor elastic effects, and plasticity is responsible for forming a lip, or bow, of material in front of the wheel (Fig. 6c). The piecewise linear and constant relationship between penetration and vertical force was also observed for different values of the elastic modulus, which only affected the range and slope of the linear portion of the response.

The reason for constant $\bar{\delta}$ at large $\bar{W}$, and the increase in $\bar{H}$ with $\bar{W}$, is the increasing size of the lip in front of the wheel (Fig. 6c). Disregarding elastic effects, the material ahead of and behind the plastically deforming region near the wheel must be at the same elevation as a consequence of plastic incompressibility and mass conservation. Incompressibility does not necessarily imply the absence of increasing $\bar{\delta}$ with increasing $\bar{W}$. That is, a steady state with the lowermost part of the wheel below the free surfaces at

the same level ahead of and behind the plastically deforming region is fully acceptable. It appears, however, that such a configuration would require a higher total force than rolling with the wheel penetrating only elastically. With reference to the minimum energy hypothesis discussed previously, this may be regarded as a plausible explanation for the absence of significant penetration in the two-dimensional problem. Neglecting small elastic volumetric strains, this also means that the volume occupied by the lip in front of the wheel equals the volume displaced plastically in the initial phase of rolling when the wheel dips into the material. The evolution of the free surface for homogeneous material is illustrated in Fig. 7. The vertical scale in Fig. 7b is exaggerated by a factor of 10 compared to the horizontal, such that the circular wheel appears as an ellipse.

In Fig. 8a, the numerical results relating $\bar{H}$ and $\bar{W}$ are compared with some approximate or exact analytic solutions presented in the literature for rigid-perfectly plastic material [18,19,21,22]. Other solutions yielding similar curves [32,33] are not plotted for clarity. All solutions predict a qualitatively similar steepening relationship, with the solutions by Collins [21,22] appearing the closest to the numerical results.

The first solution published by Collins [21] makes use of stress and velocity characteristics and is approximate in that the shape of the contact surface is taken as a chord, with the free surface also consisting of straight line segments (Fig. 8b). It also assumes no penetration, and this is supported by numerical simulations. In his earlier paper, Collins [21] provided the results of calculation taking contact angle α (Fig. 8b) to be small, although the mechanism he constructed also allows for large α. Without the small angle approximation, it can be readily shown that the horizontal and vertical forces are given by

$$\bar{W} = (2 + \pi - 2\alpha)\sin\alpha \tag{2}$$

$$\bar{H} = \left(2 + \pi - 2\alpha\right)\left(1 - \cos\alpha\right) \tag{3}$$

Eqs. (2) and (3) provide the relationship between $\bar{H}$ and $\bar{W}$ in parametric form. The small- and large-α solutions shown in Fig. 8a are significantly different, with the large-α solution being quite close to the results of the present study and the later contribution by Collins [22], in which numerical calculations were performed using the method of characteristics with a mechanism consisting of curved boundary segments. It should be noted that the curve from Collins [22] was reconstructed from graphical results, as no numerical data were provided and no closed form solution is available for the mechanism with curved boundaries.

Additional insight into the steady rolling process is provided in the next section by analyzing the evolution of the contact area and contact stresses.

5. Contact area and contact stresses

Previous results were in terms of the global variables involved in steady rolling, namely $\bar{W}$, $\bar{H}$, and $\bar{\delta}$. The forces W and H, as well as the torque about the wheel's axis of rotation (zero in this paper), are related to the distribution of contact stresses over the contact area between the wheel and underlying material.

Figure 9 gives the distribution of normal and shear stresses, denoted σ_n and σ_t respectively, over the arc of contact from three-dimensional ($\bar{b} = 0.6$) and two-dimensional ($\bar{b} = \infty$) simulations of steady rolling with $\bar{W} = 2$. Contact stresses from the three-dimensional simulation were evaluated at the wheel midplane (plane of symmetry). The shear stresses are considerably smaller than the normal stresses and are pointwise positive and negative as a result of the condition for vanishing wheel torque. The normal stresses are roughly constant over the arc of contact, with the contact angle α being larger and normal stresses being on average lower in the two-dimensional simulation than the three-dimensional simulation, due to increased material accumulation ahead of the wheel. Slight elastic rebound causes material to contact the wheel surface over a very small region behind the lowermost part of the wheel ($\theta < 0$ in Fig. 9).

Based on the distribution of contact stresses in Fig. 9 consisting of roughly constant normal stresses and small shear stresses, the average stress concept is both useful and meaningful in analysis. In steady rolling, it is natural to define average stress in terms of the resultant force Q, defined as

$$Q = \sqrt{W^2 + H^2} \tag{4}$$

and the inclined contact length h defined in Fig. 1a. Contact length h is the projected (chord) length as opposed to the arc length. Collins [21] used a similar simplification in taking the contact surface as a chord (Fig. 8b). As shown in Fig. 10a, simulations reveal that the inclination angle β (Fig. 1a) and the contact angle α are related by

$$\beta \approx \frac{\alpha}{2} \tag{5}$$

for arbitrary $\bar{W}$ in the predominantly plastic regime. The condition in Eq. (5) is equivalent to saying that the resultant force is nearly perpendicular to the chord defining *h*. In the solution by Collins [21], Eq. (5) holds by construction as opposed to being the result of analysis. With perpendicularity of the resultant force to the chord defining *h*, an appropriate definition of average normal stress *q* is

$$q = \frac{Q}{hb} \tag{6}$$

Complimentary with Eq. (6) is that average shear stress over the chord defining *h* is zero. As in previous considerations, force per unit width in the two-dimensional problem is viewed as being interchangeable with the ratio *Q*/*b* in Eq. (6). Contact length *h* in Eq. (6) is related to the contact angle α through

$$h = 2r \sin\frac{\alpha}{2} \tag{7}$$

In the remainder of this section, normalized average stress $\bar{q} = q/k$ and normalized contact length $\bar{h} = h/r$ are the operative variables. Using Eqs. (5)-(7) and several trigonometric identities, normalized forces may be expressed as

$$\bar{Q} = \bar{q}\,\bar{h} \tag{8}$$

$$\bar{W} = \bar{Q}\cos\beta \approx \bar{q}\,\bar{h}\cos\frac{\alpha}{2} = \bar{q}\,\bar{h}\sqrt{1-\frac{1}{4}\bar{h}^2} \tag{9}$$

$$\bar{H} = \bar{Q}\sin\beta \approx \bar{q}\,\bar{h}\sin\frac{\alpha}{2} = \frac{1}{2}\bar{q}\,\bar{h}^2 \tag{10}$$

In Eqs. (8)-(10), force is simply the product of $\bar{q}$ and an algebraic function of $\bar{h}$.

The relationship between $\bar{q}$ and $\bar{h}$ in steady rolling is given in Fig. 10b for $\bar{b} = 0.6$ and $\bar{b} = \infty$. It should be pointed out that $\bar{h}$ was found directly from the numerical results, whereas $\bar{q}$ was calculated, with the aid of Eqs. (4) and (6), from specified $\bar{W}$ and numerical values of $\bar{h}$ and $\bar{H}$. The basic result illustrated in Fig. 10b is that $\bar{q}$ does not substantially change as $\bar{h}$ varies. In other words, average stress is roughly a constant in Eqs. (8)-(10), and forces on the wheel vary chiefly through changing contact length. For both $\bar{b} = 0.6$ and $\bar{b} = \infty$, average stress initially increases somewhat as a function of $\bar{h}$, and at some value of $\bar{h}$, it begins to gradually decrease. The decrease in average stress with $\bar{h}$ can be attributed to inclination of the resultant force. In fact, the value of inclined average stress $\bar{q}$ is quite close to that from Hill's [30] wedge solution with wedge angle $\alpha/2$ (see inset in Fig. 10b). The wedge solution gives

$$\bar{q} = 2 + \pi - 2\alpha = 2 + \pi - 4\sin^{-1}\left(\frac{\bar{h}}{2}\right) \tag{11}$$

The expression to the right of the first equality in Eq. (11) is recognizable as the factor preceding the trigonometric function in Eqs. (2) and (3), as the solution proposed by Collins [21] is fundamentally equivalent to the wedge solution.

Fig. 10b shows that $\bar{q}$ with $\bar{b} = 0.6$ is generally higher than with $\bar{b} = \infty$. The increase in $\bar{q}$ for the three-dimensional process also agrees with what is known in the literature regarding limit loads on elastic-plastic material. That is, average stress is greater in the three-dimensional failure mechanism as compared to the two-dimensional one (cf. [34]). It is not surprising that Eq. (11) provides a better match to the results for a two-dimensional rolling wheel, as it derives from a two-dimensional solution.

In Eqs. (8)-(10), wheel forces are related to contact length, and whether contact length can be related to penetration depends crucially on the width of the wheel. This is demonstrated in Fig. 11, which shows that contact length cannot be uniquely related to penetration in the two-dimensional process. As mentioned previously, penetration in the two-dimensional process would be zero for all values of contact length in the absence of elasticity. However, contact length is fully determined by the penetration with a narrow (three-dimensional) wheel. Indeed, the authors [14-17] successfully formulated an approximate analytic method for three-dimensional steady rolling that involved use of the relationship

$$\bar{h} = \sqrt{2\bar{\delta}} \tag{12}$$

Eq. (12), also plotted in Fig. 11, is obtained through simple geometric construction by disregarding the lip of accumulated material ahead of the wheel. As the wheel becomes narrower, material accumulation tends to decrease and Eq. (12) provides a better approximation to the true contact length.

The steady rolling process bears considerable similarity to indentation. Figure 12 shows how contact length and average stress vary as a function of penetration in indentation, where indentation simulations were carried out as described in a previous paper [16]. Contact length evolves as a function of penetration in essentially the same way for the three- and two-dimensional processes, being very close to the theoretical prediction obtained by disregarding material displaced by the wheel (Fig. 12a). Aside from the relatively minor effects of inclined loading, this is the fundamental difference between indentation and steady rolling, where incompressibility in steady rolling imposes a kinematic constrain leading to very small (elastic) steady-state penetration. Fig. 12b shows that normalized average stress is very close to $2+\pi$, which is the value obtained by Prandtl [35] for a uniform load on a flat, rigid-plastic surface (Fig. 12b). Prandtl's solution is the particular case of Hill's [30] wedge solution (see Fig. 10b), when wedge angle is zero. As in rolling, it can be seen that three-dimensional effects tend to increase the average stress.

6. Conclusions

Deformation and forces predicted from three- and two-dimensional simulations of a rigid torque-free wheel rolling on plastically deforming material were assessed in detail,

considering both transient and steady rolling regimes. In particular, the dependence of wheel penetration, material-wheel contact area, and contact stress on applied wheel force were evaluated for narrow and wide three-dimensional wheel geometries as well as wheels of theoretically infinite width (cylinders), for which two-dimensional (plane strain) analysis applies. Comparison with the indentation process is also provided to show the basic similarities and differences between the indentation and steady rolling processes.

A basic conclusion from the paper is that rolling resistance (i.e., the relationship between horizontal and vertical force) is qualitatively similar whether three- or two-dimensional analysis is employed, whereas wheel penetration and material deformation can be quite different. This conclusion is especially true for narrow wheels, where induced material deformation in inherently three-dimensional and the propensity for material to displace to the sides of the wheel is entirely disregarded in two-dimensional analysis. Since previous theoretical works in the literature were based on two-dimensional formulations consisting of deformation only within the plane of wheel motion, this paper provides a reference as to potential errors arising from neglecting out-of-plane effects.

As applications involving a cylinder are relatively few in number compared to those involving a narrow wheel, the findings described in this paper are of practical relevance. In mobility applications, for instance, it is desirable to transport a weight with the least amount of effort. Results provided in this paper indicate that, for a given weight, multiple narrow wheels provide less rolling resistance than a single wide wheel. Reduced rolling resistance is, however, at the cost of increased penetration. Furthermore,

theoretical results suggest that the wheels will bury themselves in the material (i.e., penetrate unstably) at lower vertical force for a single wide wheel as compared with multiple narrow wheels. Such conclusions regarding penetration, rolling resistance, and load capacity supplement previous works on vehicle mobility (e.g., [8]).

For the von-Mises type material considered in this paper, both three- and two-dimensional results show that increasing wheel force causes a corresponding increase in contact area between the wheel and material as opposed to a significant change in average stress over that area. For a narrow wheel, material accumulation ahead of the wheel is minimal and contact area increases as a result of increased wheel penetration. For a very wide wheel, contact area increases mainly through increased accumulation, as material flow to the sides of the wheel is prohibited. Thus, penetration can be large for a narrow wheel and small for a wide wheel even though force per unit width may be the same. Horizontal force, which arises due to material exerting a horizontal force along the arc of contact, qualitatively depends on applied vertical force per unit width in the same way for narrow and wide wheels.

Acknowledgements

Financial support provided by the Shimizu Corporation is gratefully acknowledged. Computer resources were provided by the Minnesota Supercomputing Institute.

References

[1] Johnson KL. Contact mechanics. Cambridge: Cambridge University Press; 1985.

[2] Roberts WL. Cold rolling of steel. New York: Marcel Dekker, Inc.; 1978.

[3] Tselikov AI, Nikitin GS, Rokotyan SE. The theory of lengthwise rolling. Moscow: MIR Publishers; 1981.

[4] Mori K, Osakada K. Simulation of three-dimensional deformation in rolling by the finite-element method. International Journal of Mechanical Sciences 1984;26(9-10):515-525.

[5] Chen D, Bilyeu J, Walker D, Murphy M. Study of rut-depth measurements. Transportation Research Record 2001;1764:78-88.

[6] Jones R, Horner D, Sullivan P, Ahlvin R. A methodology for quantitatively assessing vehicular rutting on terrains. Journal of Terramechanics 2005;42(3-4):245-257.

[7] Shoop SA, Haehnel R, Janoo V, Harjes D, Liston R. Seasonal deterioration of unsurfaced roads. Journal of Geotechnical and Geoenvironmental Engineering ASCE 2006;132(7):852-860.

[8] Bekker MG. Introduction to terrain-vehicle systems. Ann Arbor: University of Michigan Press; 1969.

[9] Karafiath LL, Nowatzki EA. Soil mechanics for off-road vehicle engineering. Clausthal: Trans Tech Publications; 1978.

[10] Wong JY. Theory of ground vehicles. New York: Wiley; 2001.

[11] Shoop SA, Richmond PW, Lacombe J. Overview of cold regions mobility modeling at CRREL. Journal of Terramechanics 2006;43(1):1-26.

[12] Shoop SA, Kestler K, Haehnel R. Finite element modeling of tires on snow. Tire Science and Technology 2006;34(1):2-37.

[13] Li Q, Ayers PD, Anderson AB. Prediction of impacts of wheeled vehicles on terrain. Journal of Terramechanics 2007;44(2):205-215.

[14] Hambleton JP. Modeling test rolling in clay. MS thesis, University of Minnesota, Minneapolis; 2006.

[15] Hambleton JP, Drescher A. Modeling test rolling on cohesive subgrades. In: Loizos A, Scarpas T, Al-Qadi IL, eds. Advanced characterisation of pavement and soil engineering materials, Vol. 1. London: Taylor and Francis; 2007. p. 359-368.

[16] Hambleton JP, Drescher A. Modeling wheel-induced rutting in soils: Indentation. Journal of Terramechanics 2008;45(6):201-211.

[17] Hambleton JP, Drescher A. Modeling wheel-induced rutting in soils: Rolling. Journal of Terramechanics 2009;46(2):35-47.

[18] Mandel J. Résistance au roulement d'un cylindre indéformable sur un massif parfaitement plastique. In: Le frottement et l'usure. Paris: GAMI; 1967. p. 25-33.

[19] Marshall EA. Rolling contact with plastic deformation. Journal of the Mechanics and Physics of Solids 1968;16(4):243-254.

[20] Dagan G, Tulin MP. A study of the steady flow of a rigid-plastic clay beneath a driven wheel. Journal of Terramechanics 1969;6(2):9-27.

[21] Collins IF. A simplified analysis of the rolling of a cylinder on a rigid/perfectly plastic half-space. International Journal of Mechanical Sciences 1972;14(1):1-14.

[22] Collins IF. On the rolling of a rigid cylinder on a rigid/perfectly plastic half-space. Journal de Mécanique appliquée 1978;2(4):431-448.

[23] Yong RN, Fattah EA, Boonsinsuk P. Analysis and prediction of tyre-soil interaction and performance using finite elements. Journal of Terramechanics 1978;15(1):43-63.

[24] Foster WA, Johnson CE, Raper RL, Shoop SA. Soil deformation and stress analysis under a rolling wheel. In: Proceedings of the 5th North American ISTVS conference/workshop. Saskatoon, SK, Canada, May 1995:194-203.

[25] Liu CH, Wong JY. Numerical simulations of tire-soil interaction based on critical state soil mechanics. Journal of Terramechanics 1996;33(5): 209-221.

[26] Tordesillas A, Shi J. Frictionless rolling contact of a rigid circular cylinder on a semi-infinite granular material. Journal of Engineering Mathematics 2000;37(1-3):231-252.

[27] Fervers CW. Improved FEM simulation model for tire-soil interaction. Journal of Terramechanics 2004;41(2-3):87-100.

[28] Chiroux RC, Foster WA, Johnson CE, Shoop SA, Raper RL. Three-dimensional finite element analysis of soil interaction with a rigid wheel. Applied Mathematics and Computation 2005;162(2):707-722.

[29] ABAQUS Version 6.6 Documentation. Providence: ABAQUS, Inc.; 2004.

[30] Hill R. The mathematical theory of plasticity. Oxford: Oxford University Press; 1950.

[31] Petryk H. Non-unique slip-line field solutions for the wedge indentation problem. Journal de Mécanique appliquée 1980;4(3):255-282.

[32] Segal VM. Plastic contact in the motion of a rough cylinder over a perfectly plastic half-space. Mekhanika Tverdoga Tela 1971;6(3):184-189.

[33] Petryk H. Slip-line field analysis of the rolling contact problem at high loads. International Journal of Mechanical Sciences. 1983;25(4):265-275.

[34] Zhu M, Michalowski RL. Shape factors for limit loads on square and rectangular footings. Journal of Geotechnical and Geoenvironmental Engineering 2005;131(2):223-231.

[35] Prandtl L. Über die Eindringungsfestigkeit (Härte) plastischer Baustoffe und die Festigkeit von Schneiden. Zeitschrift fur Angewandte Mathematik und Mechanik 1921;1(1):15-20.

Figures

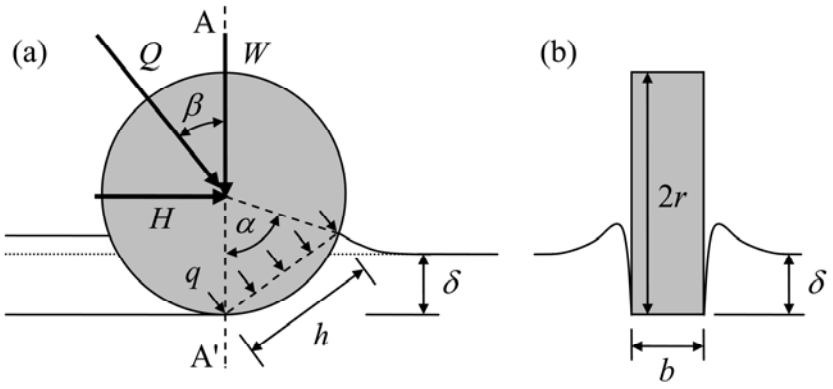

Figure 1. Schematic of three-dimensional rolling wheel on plastic material: (a) diametral plane; (b) breadthwise plane, section AA'.

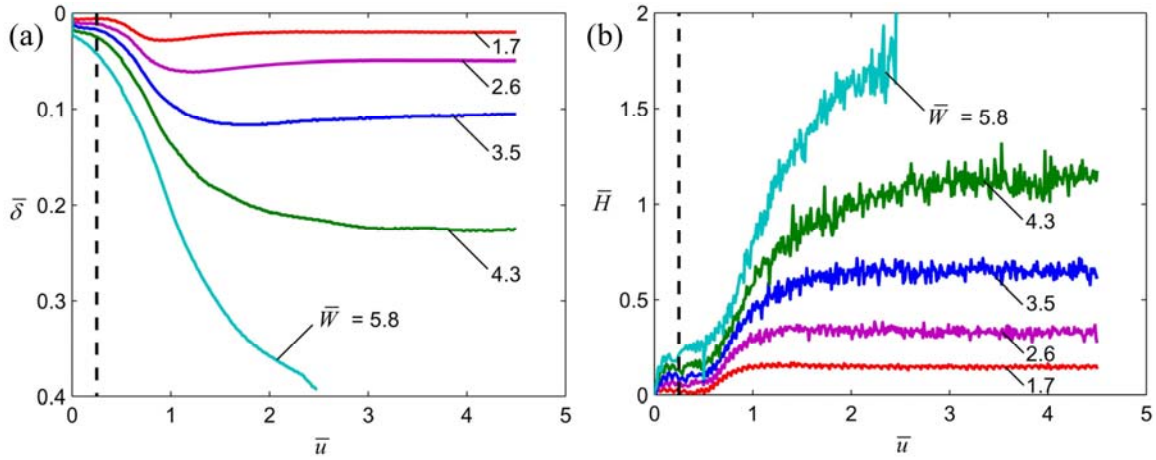

Figure 2. (a) Penetration and (b) horizontal force *vs* horizontal wheel displacement for varying vertical force ($\overline{b}$ = 0.6).

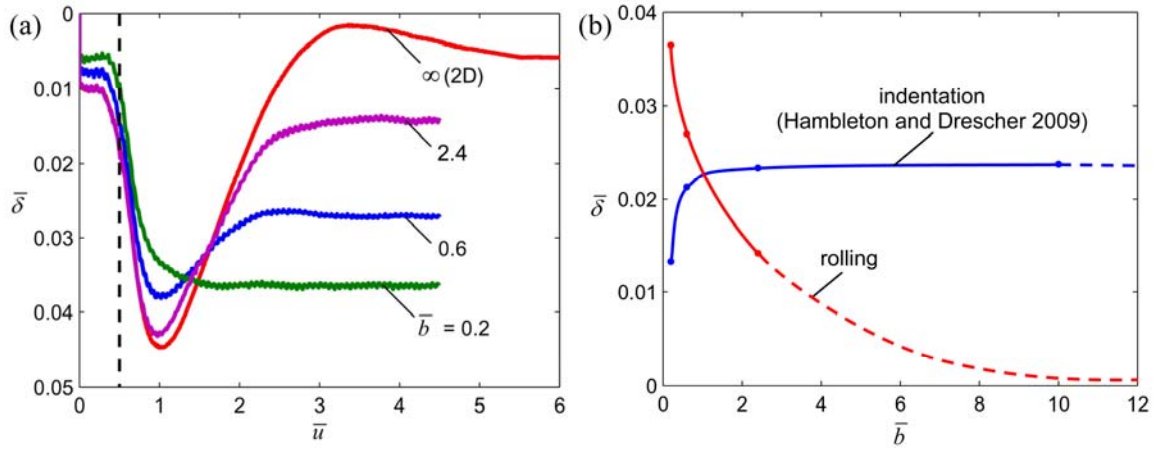

Figure 3. (a) Penetration *vs* horizontal wheel displacement with varying wheel aspect ration and (b) penetration in steady state *vs* varying wheel aspect ratio ($\overline{W}$ = 2).

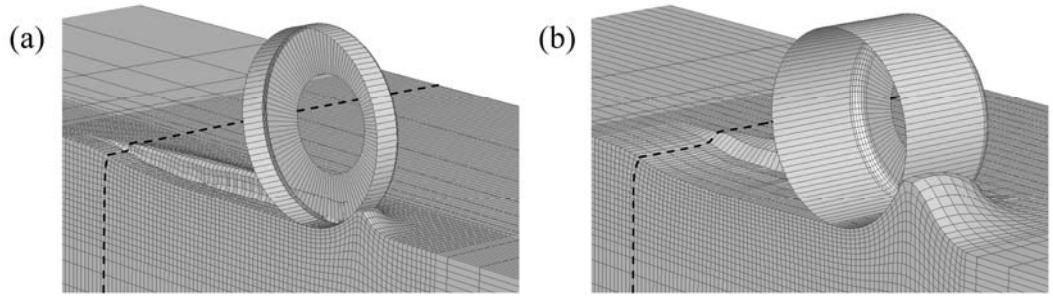

Figure 4. Final configuration from three-dimensional numerical simulation of rolling wheel ($\overline{W} = 3.75$) with (a) $\overline{b} = 0.6$ and (b) $\overline{b} = 4.8$.

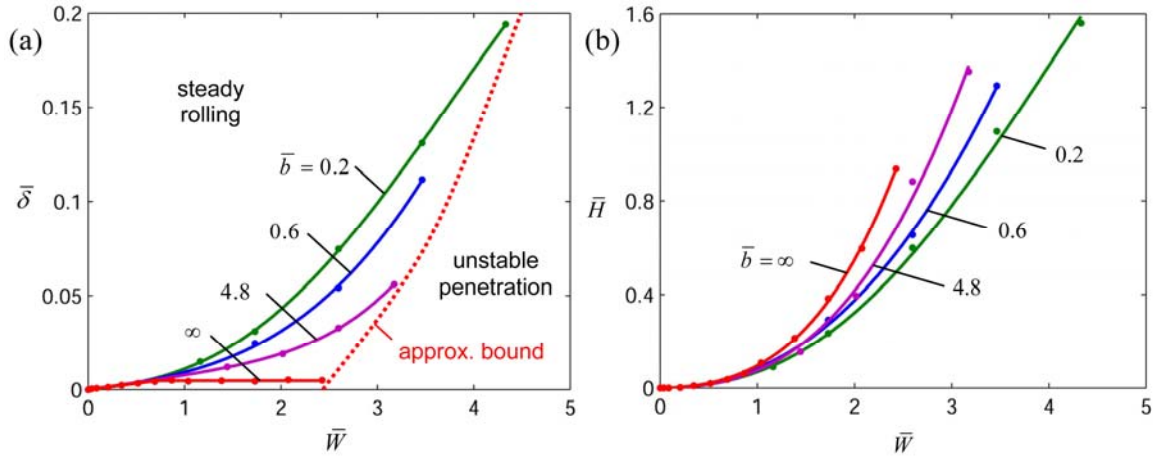

Figure 5. Response curves for steady rolling: (a) penetration *vs* vertical force; (b) horizontal force *vs* vertical force.

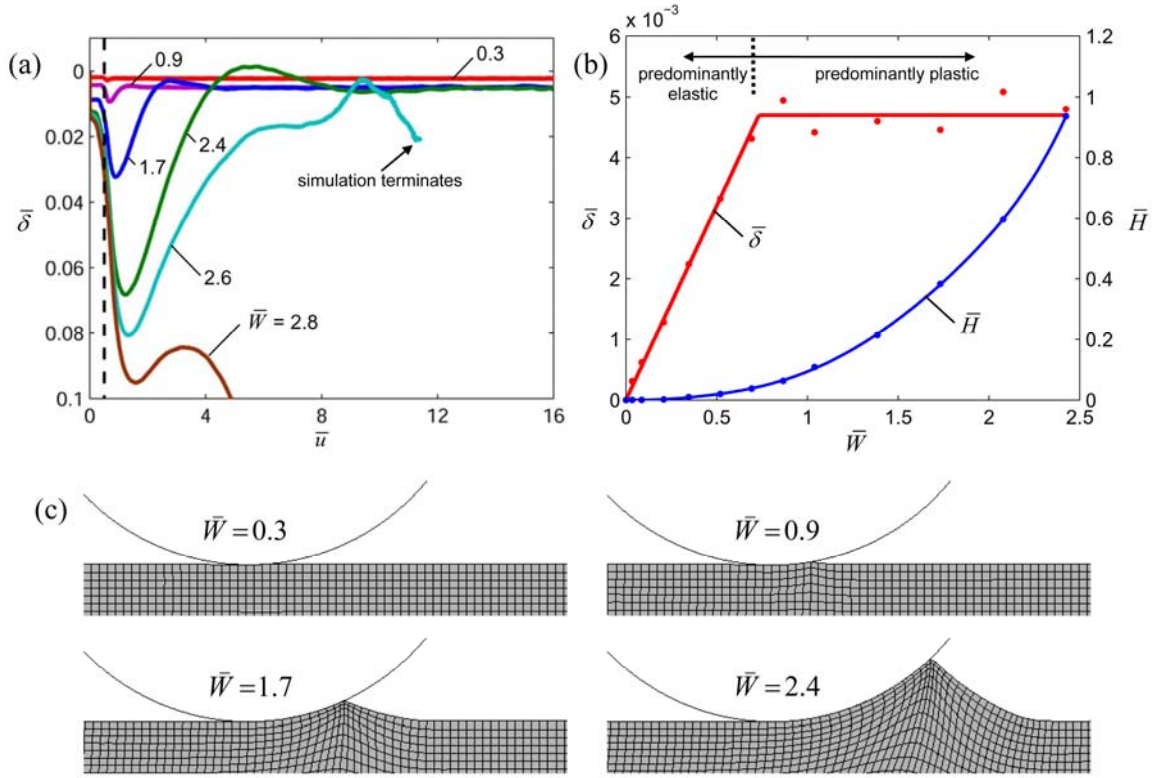

Figure 6. Cylinder rolling: (a) penetration *vs* horizontal displacement; (b) penetration and horizontal force *vs* vertical force in steady rolling; (c) geometry of plastic lip in steady rolling for varying vertical force.

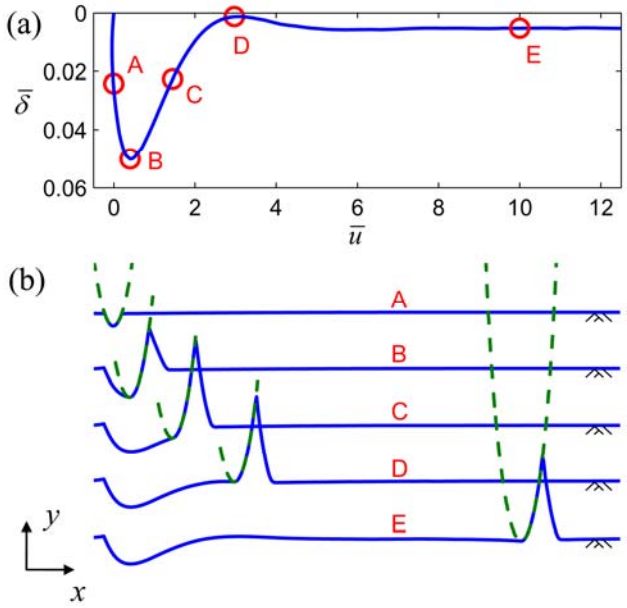

Figure 7. Cylinder rolling ($\bar{W} = 2$): (a) penetration *vs* horizontal wheel displacement; (b) evolution of free surface (surface and wheel are scaled by factor of 10 along *y*-direction).

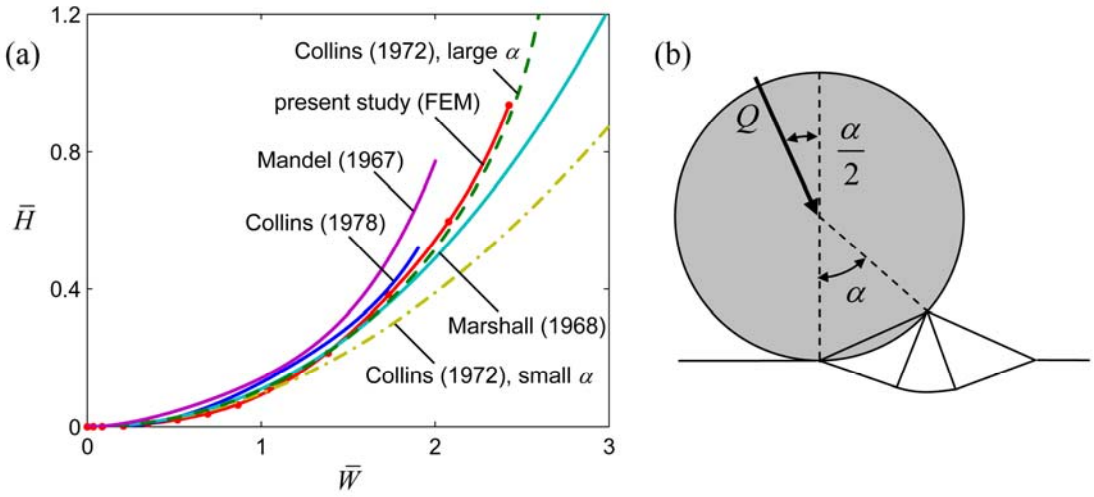

Figure 8. Comparison of numerical and analytic results for a rolling cylinder: (a) horizontal force *vs* vertical force; (b) field of characteristics after Collins [21].

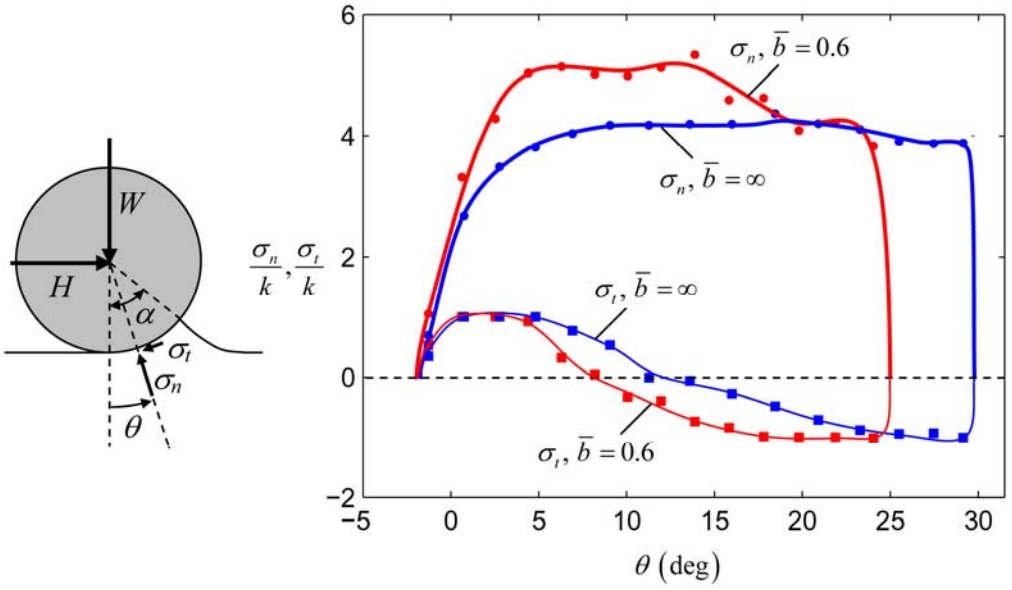

Figure 9. Contact normal and shear stresses for $\bar{W} = 2$.

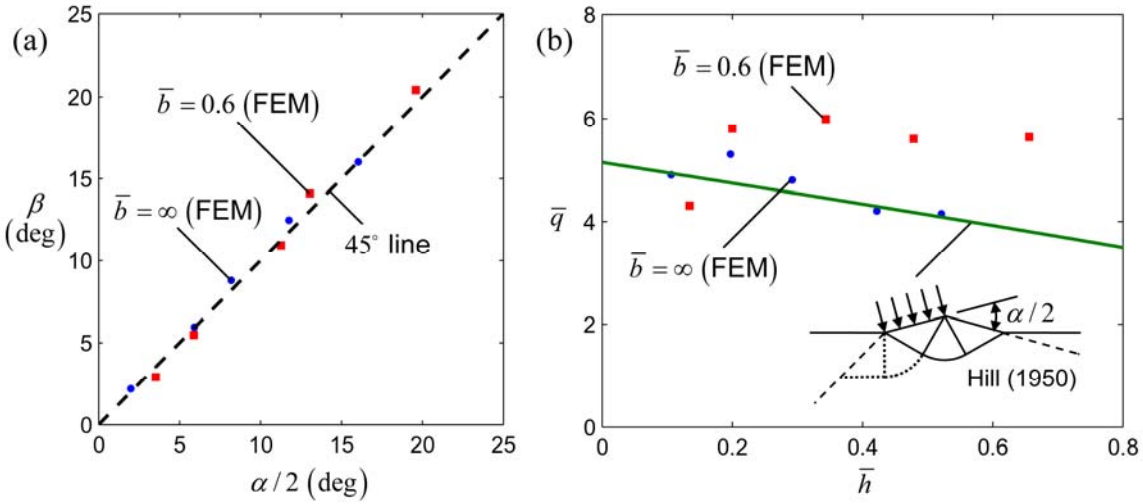

Figure 10. (a) Variation of force inclination angle β with contact half-angle $\alpha/2$ and (b) average stress *vs* contact length for steady rolling.

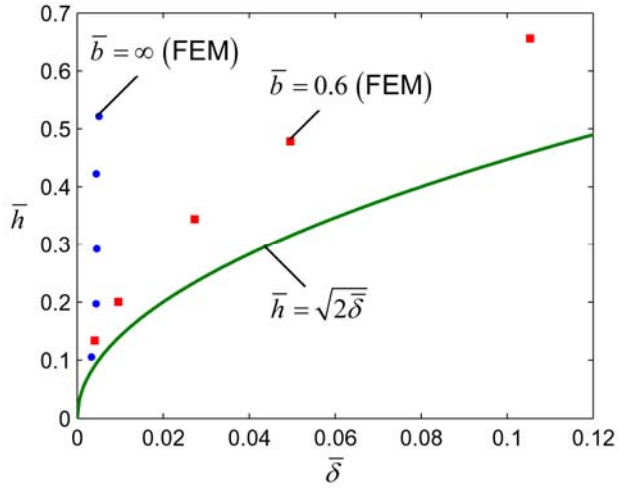

Figure 11. Contact length *vs* penetration for steady rolling.

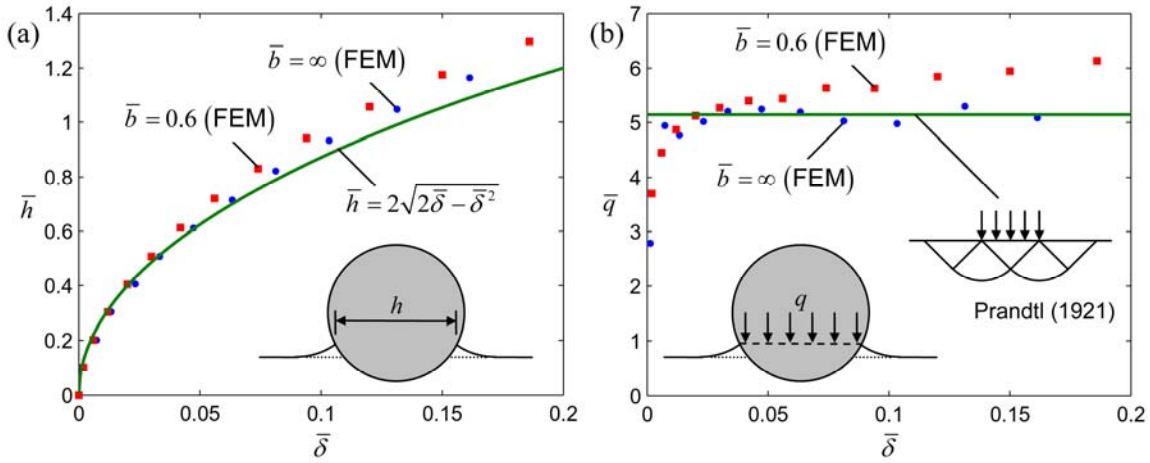

Figure 12. (a) Contact length and (b) average stress *vs* penetration for indentation process.